Letter

Discovery and Characterization of a Chemical Probe for Cyclin-Dependent Kinase-Like 2

Frances M. Bashore, Sophia M. Min, Xiangrong Chen, Stefanie Howell, Caroline H. Rinderle, Gabriel Morel, Josie A. Silvaroli, Carrow I. Wells, Bruce A. Bunnell, David H. Drewry, Navjot S. Pabla, Sila K. Ultanir, Alex N. Bullock, and Alison D. Axtman*

Read Online

ACCESS | Metrics & More | Article Recommendations | Supporting Information

ABSTRACT: Acylaminoindazole-based inhibitors of CDKL2 were identified via analyses of cell-free binding and selectivity data. Compound **9** was selected as a CDKL2 chemical probe based on its potent inhibition of CDKL2 enzymatic activity, engagement of CDKL2 in cells, and excellent kinome-wide selectivity, especially when used in cells. Compound **16** was designed as a negative control to be used alongside compound **9** in experiments to interrogate CDKL2-mediated biology. A solved cocrystal structure of compound **9** bound to CDKL2 highlighted key interactions it makes within its ATP-binding site. Inhibition of downstream phosphorylation of EB2, a CDKL2 substrate, in rat primary neurons provided evidence that engagement of CDKL2 by compound **9** in cells resulted in inhibition of its activity. When used at relevant concentrations, compound **9** does not impact the viability of rat primary neurons or certain breast cancer cells nor elicit consistent changes in the expression of proteins involved in epithelial−mesenchymal transition.

KEYWORDS: Cyclin dependent kinase-like 2, CDKL2, Protein kinase, Acylaminoindazole, Chemical probe, Epithelial−mesenchymal transition
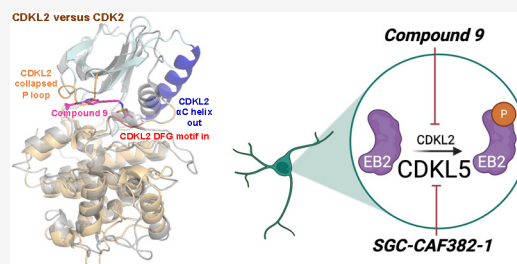
Cyclin-dependent kinase-like 2 (CDKL2, KKIAMRE, P56) is a serine/threonine kinase from the CMGC kinase group and CDKL family.[1] The CDKL family consists of CDKL1−5. Enhanced tissue expression of CDKL2 is observed in the retina and testis, but it is also nonspecifically expressed throughout the brain and in the lungs and kidneys.[2−4] CDKL2 is cytoplasmic and localizes to the nucleoplasm and centrosome in cells.[5−7] Based on characterization of animal and human cDNA clones, at least four variants of this enzyme may exist, generated by alternative splicing.[2] All putative isoforms identified from human, rabbit, and mouse cDNAs contain a common kinase domain and vary in the carboxy-termini.[2] In humans, two major transcripts were found in the adult testis, kidney, brain, and lung, and a single transcript in the fetal brain and kidney.[7]

While few publications have been published on CDKL2, some intriguing details about the biology of this kinase have been described. CDKL2 is activated in cells by treatment with epidermal growth factor.[7] As this activation does not require phosphorylation of the conserved MAP kinase dual phosphorylation motif of CDKL2, CDKL2 is not considered a functional member of the MAP kinase group.[7] While several studies have linked CDKL2 and tumorigenesis, an understanding of how CDKL2 modulates oncogenic progression is not yet understood. Reports have linked CDKL2 expression to the progression and survival of patients with kidney,[6,8]

stomach,[5,9,10] liver,[11] brain,[12] prostate,[13] and breast[14−16] cancers. CDKL2 expression is a favorable prognostic marker in glioma and renal and liver cancers.[6,8,11,12] Increased DNA methylation of CDKL2 has been observed in tissue taken from patients with liver[11,17,18] and prostate[13] cancer. In hepatocarcinomas, CDKL2 hypermethylation has been correlated with its reduced expression and cancer progression.[11]

However, high CDKL2 expression is associated with poorer survival in breast cancer.[5] Based on an orthotopic breast cancer xenograft model, this is partially driven by CDKL2 promoting primary tumor formation and spontaneous metastasis.[14] CDKL2 was identified as a regulator of epithelial−mesenchymal transition (EMT), a process associated with increased migration, metastasis, and therapeutic resistance and cells becoming stem cell-like.[5,14] Accordingly, CDKL2 expression was significantly higher in mesenchymal breast cancer cell lines, human mesenchymal stem cells, and fibroblasts when compared to epithelial breast cancer cell
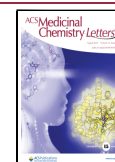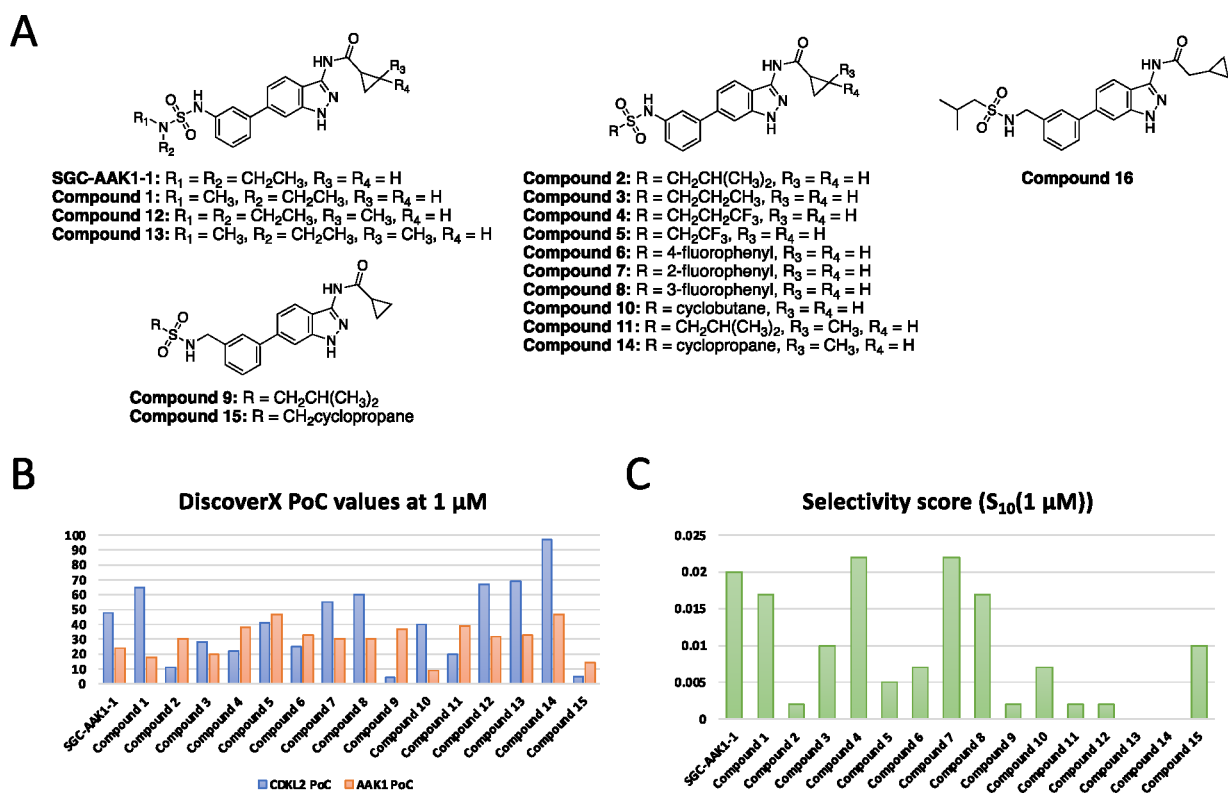
Figure 1. Structures and data for acylaminoindazole analogues. (A) Structures of all acylaminoindazole analogues considered herein. (B) Comparison of DiscoverX percent of control (PoC) values at 1 μM for CDKL2 and AAK1. (C) Selectivity score for each analogue when analyzed versus 403 wild-type human kinases at 1 μM.

lines.[14] In contrast, it was reported that CDKL2 is hypermethylated and its expression downregulated in HER2+ breast cancer tissues, suggesting that CDKL2 upregulation inhibits cancer progression.[15] These results support that the role of CDKL2 in breast cancer is not fully understood. Similarly, based upon analysis of patient samples, the literature is mixed on the role of CDKL2 in gastric cancer, with one group reporting that high CDKL2 mRNA level predicts shorter overall survival[9] and two other groups reporting that loss of CDKL2 predicts poor prognosis.[5,10]

Beyond cancer, CDKL2 plays a role in development, supporting behavior control, emotion, and cognitive functions required to acquire spatial and contextual learning.[4,19] CDKL2 is also responsive to viral infection. HSV-2 infected HeLa cells demonstrated reduced expression of CDKL2, which was suggested to impact processes such as apoptosis and cell cycle in these cells.[20] With better tools, including a small molecule chemical probe, additional studies can be performed to further characterize how CDKL2 modulates other disease-relevant pathways.

Crystal structures of the CDKL2 kinase domain bound to TCS 2312 (PDB 4BBM) and to CDK1/2 Inhibitor III (PDB 4AAA) have been solved.[21] These structures revealed that CDKL2 has a distinct C-terminal αJ helix that is also found in CDKL3 but not in other CDKL family members.[21] The motif occludes the recruitment site for MAPK substrates, supporting the idea that CDKL family members mediate disparate protein interactions when compared to MAPKs.[21] The αJ region was also found to be essential for CDKL2 function and its deletion significantly reduced CDKL2 activity. The ligand-bound structures harbored an inactive αC-out conformation and ligand binding was stabilized by a collapsed P-loop

conformation.[21] Interestingly, an active kinase conformation was also compatible with binding of CDK1/2 Inhibitor III and thus inhibitor interactions are not solely responsible for the inactive conformation observed.[21] The structures of other CDKL family members displayed characteristics of active kinases, making CDKL2 structurally unique.[21]

Importantly, the compounds that were cocrystallized with CDKL2 are not selective for CDKL2, but rather broad-spectrum ATP-competitive kinase inhibitors. While these do not represent the only kinases inhibited by the compounds, TCS 2312 is sold as a CHK1 inhibitor, while CDK1/2 Inhibitor III is often used to inhibit CDK1 and CDK2. No potent and selective small molecule inhibitors of CDKL2 have been published. Such a compound would represent a powerful tool that would aid in deciphering the biological roles of CDKL2.

In search of a high-quality CDKL2 inhibitor, we reviewed our kinome-wide screening data. We identified the acylaminoindazoles as a promising chemical series with robust CDKL2 binding affinity. The acylaminoindazoles were the source of our AAK1/BMP2K probe, SGC-AAK1−1 (Figure 1A).[22] Because these compounds were known to be AAK1 active, the first step was to compare the cell-free binding affinity at 1 μM of each analogue for AAK1 and CDKL2 (Figure 1B). The kinome-wide selectivity of each compound at 1 μM ($S_{10}(1$ μM)) was considered in parallel (Figure 1C). The S_{10} score expresses selectivity and corresponds with the percent of the kinases screened that bind with a percent of control (PoC) value <10. A lower PoC value (closer to zero) correlates with higher binding affinity. While kinases bind compounds with different PoC ranges, a PoC < 10 is universally treated as indicative of high affinity binding. When calculating a

Table 1. Potency and Selectivity Data for Acylaminoindazole Analogues

cmpd	CDKL2 PoC	AAK1 PoC	$S_{10}(1\ \mu M)$ score[a]	no. kinases with PoC < 10[b]	CDKL2 radiometric enzymatic assay IC_{50} (nM)	CDKL2 NanoBRET assay IC_{50} (nM)
SGC-AAK1-1	48	24	0.02	8		>10000
1	65	18	0.017	7		
2	11	30	0.002	1		
3	28	20	0.01	4		
4	22	38	0.022	9		
5	41	47	0.005	2		
6	25	33	0.007	3		1200
7	55	30	0.022	9		
8	60	30	0.017	7		
9	4.3	37	0.002	1	230	460
10	40	9.2	0.007	3		
11	20	39	0.002	1		
12	67	32	0.002	1		
13	69	33	0	0		>10000
14	97	47	0	0		>10000
15	5	14	0.01	4	450	700
16	NT[c]	NT	NT	NT		>10000

[a]S_{10} (1 μM): percentage of screened kinases with PoC < 10 at 1 μM. [b]PoC: percent of control values determined at 1 μM via DiscoverX *scanMAX* profiling. [c]NT: not tested.

selectivity score, only the 403 wild-type human kinases in the DiscoverX *scanMAX* panel are considered. Binding affinity and kinome-wide selectivity scores for all analogues in Figure 1 are included in Table 1. Most of these compounds were exemplified in our campaign to identify an AAK1/BMP2K probe.[22]

Data in Table 1 and Figure 1B demonstrated that nearly all compounds bind with modest affinity to AAK1 (PoC 10−50 at 1 μM). Because this AAK1 affinity in the DiscoverX binding assay corresponded with submicromolar activity in the AAK1 NanoBRET assay,[22] we hypothesized that most of these compounds are efficacious inhibitors of AAK1. Turning our attention to CDKL2 affinity, we noted that nine acylaminoindazole analogues bound to CDKL2 with PoC > 35. Of the remaining six analogues, only two demonstrated CDKL2 PoC < 10: compounds 9 and 15. From a structural standpoint, these two analogues were unique from the other analogues in their inclusion of a methylene space between the phenyl ring and sulfonamide (Figure 1A). Both analogues were prioritized for follow-up.

As shown in Table 1 and Figure 2, both compounds inhibited CDKL2 in a radiometric enzymatic assay with IC_{50} values <500 nM. Compounds 9 and 15 were next evaluated in the CDKL2 NanoBRET assay to gauge their ability to engage CDKL2 in cells, yielding an IC_{50} value of 460 nM for compound 9 and 700 nM for compound 15 (Table 1, Figures 2 and Supporting Information, Figure S1). The in-cell potency of compound 9 motivated a deeper dive to confirm its kinome-wide selectivity. As shown in Figure 2B, when broadly profiled against 403 wild-type human kinases compound 9 only bound one kinase with PoC < 10, supporting its selectivity score ($S_{10}(1\ \mu M)$ = 0.002) in Table 1. Nine additional kinases demonstrated a PoC < 40 in this broad profiling effort (Figure 2C). To determine whether binding resulted in inhibition of kinase activity, radiometric enzymatic assays were executed to evaluate compound 9 versus all nine kinases. This effort narrowed the kinases inhibited by compound 9 to three: CDKL2, BMP2K, and AAK1. We previously documented the activity of acylaminoindazoles on AAK1 and BMP2K[22] and

Compound 9
CDKL2 chemical probe

$S_{10}(1\ \mu M)$ = 0.002
2 kinases with <10% control
(one is a mutant kinase)

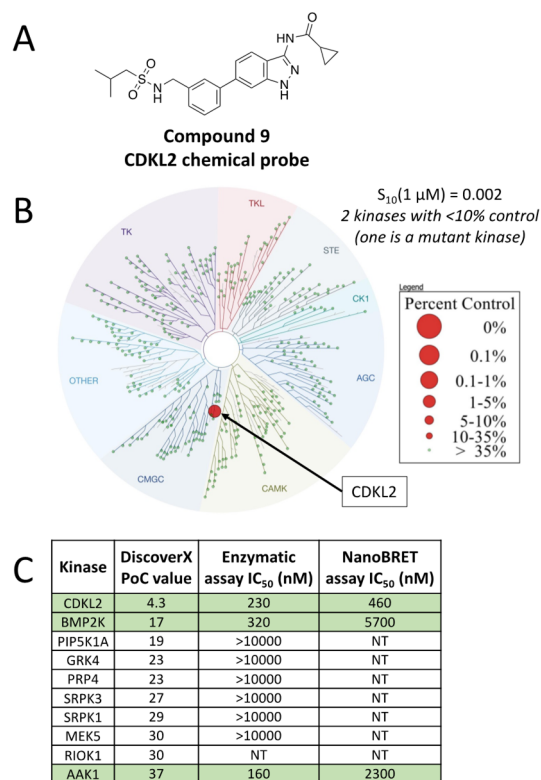| Kinase	DiscoverX PoC value	Enzymatic assay IC_{50} (nM)	NanoBRET assay IC_{50} (nM)
CDKL2	4.3	230	460
BMP2K	17	320	5700
PIP5K1A	19	>10000	NT
GRK4	23	>10000	NT
PRP4	23	>10000	NT
SRPK3	27	>10000	NT
SRPK1	29	>10000	NT
MEK5	30	>10000	NT
RIOK1	30	NT	NT
AAK1	37	160	2300

Figure 2. Structure, potency, and kinome-wide selectivity data related to CDKL2 chemical probe (compound 9). (A) Structure of compound 9. (B) Kinome dendrogram that illustrates nonmutant kinases that bind with PoC < 10 when compound 9 was screened at 1 μM in the DiscoverX *scanMAX* panel. (C) Data for all human wild-type kinases in the DiscoverX *scanMAX* panel that bound with a PoC < 40 when compound 9 was screened at 1 μM (column 2), enzymatic IC_{50} values generated when compound 9 was evaluated in each kinase radiometric enzymatic assay (column 3), and NanoBRET IC_{50} values generated when compound 9 was evaluated in each kinase NanoBRET assay (column 4). PoC = percent of control.
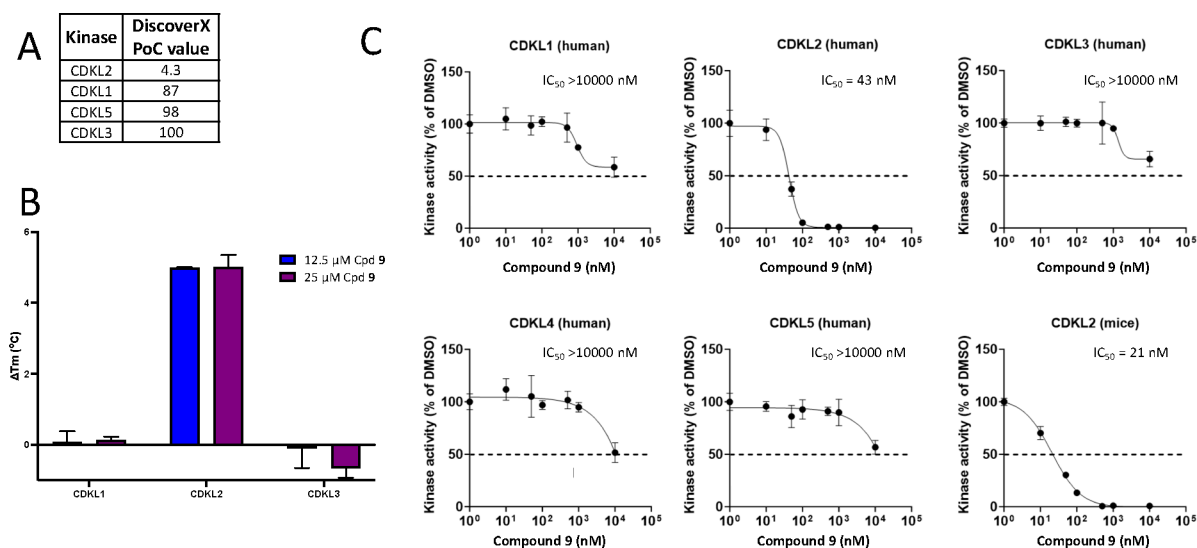
Figure 3. Data that supports the selectivity of CDKL2 chemical probe (compound **9**) within the CDKL family. (A) DiscoverX PoC values generated using the available CDKL family binding assays and screening at 1 μM of compound **9**. (B) Thermal shift assay data for compound **9** when evaluated versus CDKL1, CDKL2, and CDKL3 kinase domains. (C) In vitro kinase assay results for compound **9** when evaluated versus full-length human CDKL1−5 and murine CDKL2 and the ADP-Glo assay was used as a readout. PoC = percent of control; Cpd = compound.

this activity was maintained for compound **9** in cell-free assays. Next, engagement of AAK1 and BMP2K by compound **9** in cells was evaluated. This compound was found to have higher affinity for CDKL2 than it does for AAK1 and BMP2K in cells (Figure 2C). Truncated versions of AAK1 (1−353) and BMP2K (1−367) and full-length CDKL2 were employed in the radiometric enzymatic assays, while full-length versions of all three kinases were used in the NanoBRET assays (Figure 2C). The differences in protein used for AAK1 and BMP2K in each assay could, in part, explain the distinct results observed in the radiometric enzymatic versus NanoBRET assays. CDKL2, AAK1, and BMP2K also have different Km values for ATP, such that CDKL2 binds ATP with much lower affinity. This also explains the more significant shift in IC$_{50}$ values for AAK1 and BMP2K when moving from cell-free to NanoBRET assays.

The selectivity of compound **9** within the CDKL family was further probed. The PoC data for most of this family was collected when compound **9** was profiled in the DiscoverX scanMAX panel at 1 μM (Figure 3A). Compound **9** only demonstrated appreciable binding affinity to CDKL2 in these assays. The kinase domains of CDKL1, CDKL2, and CDKL3 were next employed in thermal shift assays with increasing concentrations of compound **9**. A dose-dependent change in the melting temperature (ΔTm) of CDKL2 was observed in the presence of this compound, while the ΔT_{m} of neither CDKL1 nor CDKL3 was perturbed by compound **9** (Figure 3B). Finally, in vitro kinase assays, using the ADP-Glo assay to readout inhibition of activity, were executed to evaluate whether compound **9** inhibits the activity of human and/or mouse forms of CDKL family members (Figure 3C). Substrate phosphorylation was not inhibited at concentrations up to 10 μM of compound **9** for CDKL1, CDKL3, CDKL4, or CDKL5. Substrate phosphorylation by the human and mouse forms of CDKL2, however, was inhibited with IC$_{50}$ values of 43 nM and 21 nM, respectively. The perceived shift in IC$_{50}$ values between the CDKL2 radiometric enzymatic assay (Figure 2C) and the CDKL2 in vitro kinase assays (Figure 3C) could be due, in part, to the difference in concentration of ATP used in each

assay, 200 μM for the radiometric enzymatic assay and 50 μM for the in vitro ADP-Glo kinase assay. Slightly different constructs were also used in each assay. The higher concentration of ATP used in the radiometric enzymatic assay provides more competition for binding to the same site as compound **9**, resulting in a comparatively elevated IC$_{50}$ value in this assay. Overall, however, the trends are the same and compound **9** is a verified, potent inhibitor of CDKL2 activity.

With a CDKL2 probe candidate identified within the acylaminoindazole series we next sought a suitable negative control compound. To meet criteria, a negative control candidate must be structurally similar to the chemical probe but lack CDKL2 inhibitory activity. A combination of the CDKL2 affinity in the DiscoverX assay and kinome-wide selectivity was considered when choosing potential candidates (Table 1). Accordingly, compounds **6**, **13**, **14**, and SGC-AAK1−1 were analyzed in the CDKL2 NanoBRET assay. Gratifyingly, SGC-AAK1-1 was found to demonstrate an IC$_{50}$ > 10 μM for CDKL2 in cells (Supporting Information, Figure S2). This makes SGC-AAK1−1 a complementary molecule to use in concert with compound **9** to tease apart cellular phenotypes resulting from AAK1/BMP2K inhibition versus those from CDKL2 inhibition when compound **9** is dosed at concentrations exceeding 1 μM. While compounds **13** and **14** were found to lack CDKL2 affinity in cells (Supporting Information, Figure S2), the chiral center on the cyclopropane ring made us less enthusiastic about these compounds and motivated preparation of a more suitable negative control based upon our established structure−activity relationships. Compound **16** (Figure 1) was next designed as a putative negative control compound. When compared to compound **9**, only one part of the molecule was modified. A methylene spacer was placed between the carbonyl and cyclopropyl ring on compound **9** to furnish compound **16**. Once prepared, compound **16** was evaluated in the CDKL2, AAK1, and BMP2K NanoBRET assays. It was found to lack affinity for all these kinases (IC$_{50}$ > 10 μM, Supporting Information, Figure S3) and thus was selected as an appropriate negative control,
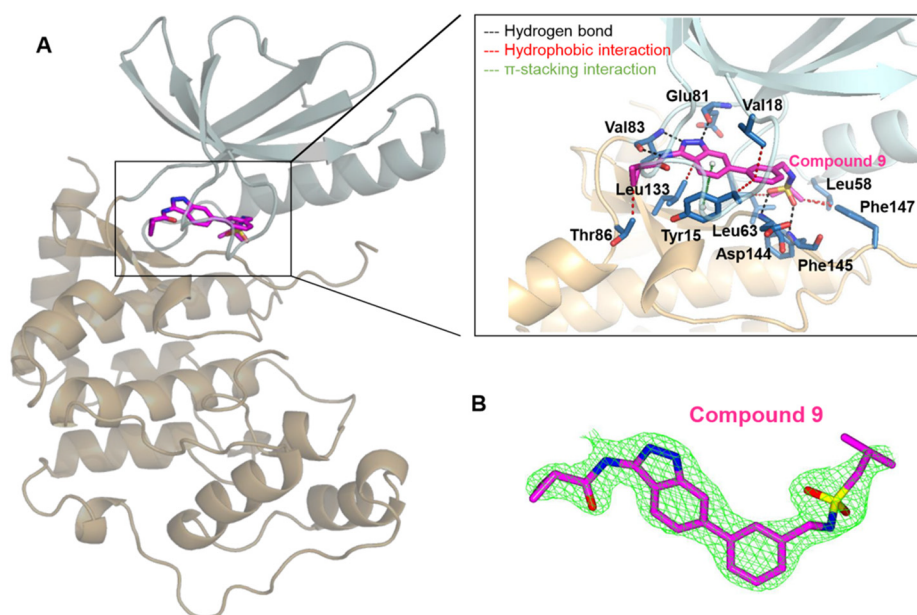
Figure 4. Cocrystal structure of CDKL2 with compound **9** (PDB 8S6I). (A) Overview of CDKL2 with compound **9**. N- and C-terminal lobes colored in pale cyan and light orange, respectively. Compound **9** (magentas sticks) binds to the active site between the two lobes. (Inset) Interactions of compound **9** with CDKL2. Black dashed lines: hydrogen bonds (Glu81, Val83, Asp144, and Phe145); red dashed lines: hydrophobic interactions (Tyr15, Val18, Leu58, Leu63, Thr86, Leu133, and Phe147); green dashed lines: π-stacking interaction (Tyr15). Interactions mapped using Protein−Ligand Interaction Profiler (PLIP). (B) mFo-DFc omit electron density map for compound **9**. The green mesh represents electron density of compound **9** at 2.0σ (CCP4 molecular graphics).

differing only by a single methylene, to be used alongside compound **9**.

Structural studies were employed to understand the binding mode and rationalize the selectivity of compound **9** for CDKL2. A cocrystal structure of compound **9** bound to CDKL2 was solved (Figure 4, Supporting Information, Table S1) and interactions mapped using Protein−Ligand Interaction Profiler (PLIP).[23] This structure shows a collapsed P-loop enveloping and stabilizing the binding of compound **9** and an αC-out, DFG-in type conformation. While the compounds are structurally very different, this binding mode is similar to the previously discussed crystal structure with TSC 2312 (PDB 4BBM) and distinct from the CDKL2 structure with CDK1/2 Inhibitor III (PDB 4AAA).[21] Like TSC 2312, compound **9** harnesses the inactive αC-out conformation that is unique to CDKL2 versus other CDKL family members.

Comparison of the structure of the AAK1/BMP2K probe bound to BMP2K (PDB 5I3R) to this new CDKL2 cocrystal structure shows that the conserved nitrogens of the acylaminoindazole core make key hydrogen bonds with Glu131 and Cys133 in BMP2K[22] and Glu81 and Val83 in CDKL2. These hydrogen bonds anchor the two compounds in similar orientations to the kinase hinge region in the respective active sites. The pendant aryl ring of compound **9** is accommodated by a large hydrophobic region of the ATP-binding site, which is common to BMP2K as well.[22] Compound **9** bears a sulfonamide that hydrogen bonds with Phe145 and Asp144 in the DFG motif. The methylene inserted between the pendant aryl ring and sulfonamide is essential in the placement of this sulfonamide in proximity to the key residues mentioned and for hydrophobic interactions with Phe147. Its importance is supported by the CDKL2 affinity of compounds **9** and **15** versus that of analogues that lack the methylene spacer (Table 1). Finally, comparison of the BMP2K and CDKL2 structures helps explain the selectivity

of compound **9** for CDKL2. The larger hydrophobic pocket in CDKL2 can enclose the longer sulfonamide side chain whereas the same pocket in BMP2K, and AAK1 by analogy given the highly homologous sequence, is smaller and would introduce steric clash when compound **9** is bound. The ATP-binding sites of other kinases are similarly unlikely to accommodate this sulfonamide, precluding their binding to compound **9** with high affinity and imparting the kinome-wide selectivity we observe.

The hydrophobic pocket that accommodates the sulfonamide, however, is large. Thus, analogues with smaller alkyl sulfonamides (**2**−**5** and **10**) bind in the DiscoverX CDKL2 assay (Table 1, CDKL2 PoC 11−41). These compounds are proposed to not encounter steric clash but also not benefit from the key hydrogen bonds with Glu81 and Val83 because they are positioned too far from these residues. Compounds bearing an aryl sulfonamide with an *ortho-* (**7**) or *meta-*fluorine (**8**) are weaker binders (Table 1, CDKL2 PoC 55−60), while the *para-*fluorinated phenyl sulfonamide (**6**) demonstrates slightly higher affinity for CDKL2 (Table 1, CDKL2 PoC 25). The pocket tolerates these larger rings and the DiscoverX CDKL2 PoC values support that the *para-*fluorine may be positioned to make additional interactions that the *ortho-* and *meta-*fluorine cannot. Finally, SGC-AAK1−1 and compound **1** are weaker binders to CDKL2 (Table 1, CDKL2 PoC 48−65). Because the sulfonamides on these two compounds are not significantly larger than those on other analogues, the added nitrogen and/or the branching (two R groups) could lead to unfavorable interactions with the binding pocket. The solved structure of compound **9** shows that the space around the cyclopropane ring in compound **9** is limited. Thus, modification of and near the cyclopropane ring is likely to perturb key interactions with Glu81 and Val83 due to steric clash and forced repositioning of analogues in the CDKL2 ATP-binding site. This finding provides rationale for why
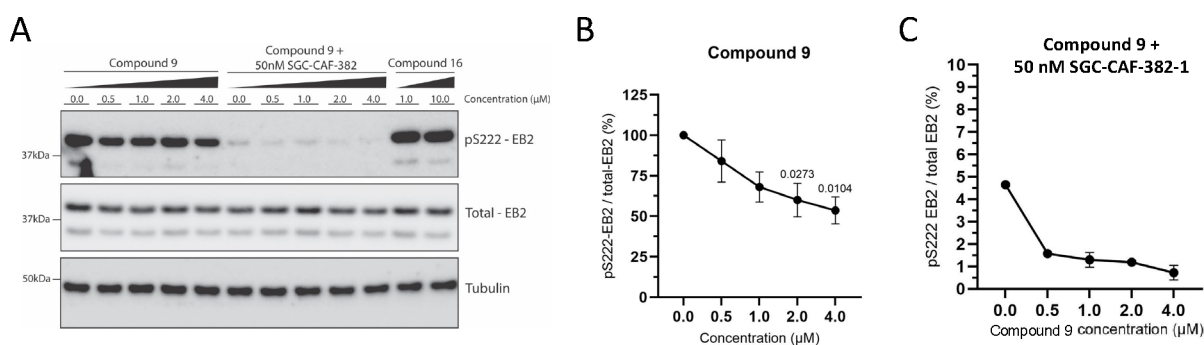
Figure 5. Western blot analyses of pS222-EB2 in rat primary neurons after 1 h treatment with compound **9**, SGC-CAF382-1, compound **9** + SGC-CAF382-1, or compound **16**. (A) Representative blot from a single replicate, replicate two in Supporting Information, Figure S4. (B) Quantification of pS222-EB2 normalized to total EB2 for compound **9** treatment, $n = 4$. Error bars represent SEM. One-way ANOVA test: p-value = 0.0191. (C) Quantification of pS222-EB2 normalized to total EB2 for compound **9** + SGC-CAF382-1 treatment, $n = 2$. Error bars represent SEM.

analogues bearing a methylated cyclopropyl ring (**11**, **12**, **13**, **14**) and the deeper projecting negative control (**16**) lack affinity for CDKL2.

With a potent and selective CDKL2 chemical probe in hand, we next evaluated its impact on downstream signaling. The Ultanir lab recently reported that CDKL2 phosphorylates microtubule end binding protein 2 (EB2) at Ser222 in HEK293T cells, primary neurons, and *in vivo*.[24] This finding motivated examination of the response of rat primary neurons to treatment with compound **9**. It is important to note, however, that CDKL5 is responsible for approximately 80% of EB2 phosphorylation.[24] Because CDKL5 is not inhibited by our compound, we expected to see a maximal 20−25% reduction of EB2 phosphorylation by the CDKL2 probe. We evaluated a CDKL5 chemical probe (SGC-CAF382−1) in parallel at a concentration (50 nM) where ∼80% reduction in EB2 phosphorylation was previously observed.[25] Neurons were treated with increasing concentrations of compound **9** alone or 50 nM of SGC-CAF382−1 with increasing concentrations of compound **9** to explore whether these two compounds could completely inhibit EB2 phosphorylation when dosed together. Negative control compound **16** was evaluated in parallel to explore chemotype-induced effects on EB2 phosphorylation. As shown in Figure 5 and Supporting Information, Figure S4, compound **9** completely suppressed the CDKL2-mediated EB2 phosphorylation in a dose-dependent manner following 1 h exposure of rat primary neurons. Total EB2 expression was not impacted. In contrast, negative control compound **16** did not perturb EB2 phosphorylation or total EB2 expression at concentrations up to 10 μM. The concentration at which EB2 phosphorylation is inhibited by compound **9** corresponds well with its IC_{50} value in the CDKL2 NanoBRET assay (460 nM). This result confirmed that CDKL2 inhibition by compound **9** disrupts CDKL2-mediated downstream signaling in rat primary neurons. The more significant reduction of EB2 phosphorylation at concentrations >1 μM is likely due to inhibition of off-target kinases that influence this process. Treatment of rat neurons with SGC-CAF382−1 alone resulted in a robust reduction in EB2 phosphorylation (∼95%). The codosing experiments with SGC-CAF382−1 confirmed that EB2 phosphorylation can be completely suppressed (∼98.5%) when CDKL5 and CDKL2 are both inhibited.

As mentioned, CDKL2 is a regulator of epithelial−mesenchymal transition (EMT), a process that can accelerate cancer progression.[5,14] It was reported that shRNA directed at

CDKL2 in breast cancer, specifically human mammary gland epithelial (HMLE) cells, decreased protein expression of vimentin and N-cadherin and mRNA levels of ZEB1 and CD44.[14] Rather than HMLE cells, we selected an epithelial (MCF-7) and mesenchymal (MDA-MBA-231) breast cancer cell line with known CDKL2 expression at the mRNA level[14] to probe whether these same responses could be recapitulated using our CDKL2 chemical probe. When these cells were treated in dose−response format with 1, 5, or 10 μM of compound **9** for 24, 48, or 72 h, no reproducible impact was observed with respect to the protein expression of CD44, ZEB1, or β-catenin (Supporting Information, Figure S5). Furthermore, when exposed to the same concentrations and time course, protein expression of E-cadherin was not altered in MCF-7 cells and vimentin in MDA-MB-231 cells. Results were inconsistent and often compounds **9** and **16** elicited a nearly identical response in these studies. We were not able to pharmacologically modulate expression of the selected EMT proteins using compound **9** at concentrations where it is CDKL2 active in cells based on NanoBRET and Western blot data. While it has become commonplace to verify small molecule inhibition results with genetic methods (siRNA or shRNA) and vice versa with the expectation that the two phenotypes will align, this is not always the case. Specific examples are sparse because these results are misinterpreted as a lack of specificity for the small molecule. Examples, however, have been published and reviewed for the Aurora B kinases and class IA PI(3)K family of lipid kinases.[26] One suggested interpretation of this discrepancy in phenotypes when using genetic and pharmacological methods is that the kinase could be playing a scaffolding function and its protein−protein interactions are only effectively disrupted by si/shRNA treatment but not by a small molecule.[26]

At a biologically relevant concentration (1 μM), we also noted that CDKL2 inhibition by compound **9** did not impact the viability of MCF7 or MDA-MB-231 cells when treated for 48 h (Supporting Information, Figure S6). A similar lack of toxicity was observed when a patient derived xenograft (PDX) model of triple-negative breast cancer (TU-BcX-4IC cells)[27] was treated in dose−response format with compound **9** (Supporting Information, Figure S6). TU-BcX-4IC cells, which were confirmed by RT-qPCR to express CDKL2, were originally derived from a patient with metaplastic triple-negative breast carcinoma, one of the most aggressive and dangerous breast cancer subtypes. Versus immortalized cell

lines, PDX-derived cell lines more accurately mimic the behavior of actual tumor cells in patients.[28] Like MDA-MB-231 cells, TU-BcX-4IC cells did not display significant changes in morphology, total area, or average cell size at 1 μM (Supporting Information, Figure S6).

We have described the evaluation of a series of acylaminoindazoles as CDKL2 inhibitors. Analyses of binding and kinome-wide selectivity data for these compounds enabled selection of compound **9** as our CDKL2 chemical probe. This compound demonstrated inhibition of CDKL2 enzymatic activity in cell-free assays and nearly equivalent engagement of CDKL2 in cells. Extensive selectivity screening, including evaluation of binding and inhibition of putative off-target kinases, has verified that compound **9** inhibits few kinases. In enzymatic assays, this compound inhibits CDKL2, AAK1, and BMP2K with nearly equivalent IC_{50} values. In cells, however, it is a higher affinity binder to CDKL2 and demonstrates a modest 5−12-fold enhanced binding affinity for CDKL2 when compared to AAK1 and BMP2K. This provides a cautionary note: compound **9** should be used at concentrations of ≤ 1 μM in cells to avoid perturbation of AAK1 and BMP2K. We suggest that our designed negative control, compound **16**, and SGC-AAK1−1 are used in tandem with compound **9** in experiments designed to probe CDKL2-mediated biology. Structural studies helped illuminate key interactions of our CDKL2 chemical probe with the ATP-binding site and rationalize potency trends within the acylaminoindazole series. Comparison of the CDKL2 cocrystal structure with compound **9** to that of SGC-AAK1−1 bound to BMP2K generated hypotheses about the selectivity of compound **9** for CDKL2 when screened broadly. Inhibition of downstream signaling without an associated impact on viability was observed when rat primary neurons were treated with compound **9**, supporting that binding to CDKL2 in cells inhibited kinase activity. The viability of breast cancer cells was also not affected when treated with the probe pair. Finally, we found that compound **9** does not phenocopy CDKL2 shRNA results related to EMT nor alter the expression of the specific proteins involved in this process in the cell lines, concentrations, and time points that we probed.

■ ASSOCIATED CONTENT

Ⓢ Supporting Information

The Supporting Information is available free of charge at https://pubs.acs.org/doi/10.1021/acsmedchemlett.4c00219.

> Synthetic schemes, NanoBRET assay curves, Western blot replicates, viability results, X-ray crystallographic data, and experimental details, including synthetic schemes and characterization of key compounds, protocols for selectivity screening and biological assays, and crystallographic details. (PDF)

Accession Codes

The PDB accession code for the X-ray cocrystal structure of CDKL2 + **9** is 8S6I. The PDB accession code for the X-ray cocrystal structure of CDK2 in the TOC graphic is 1QMZ.

■ AUTHOR INFORMATION

Corresponding Author

Alison D. Axtman − *Structural Genomics Consortium (SGC), UNC Eshelman School of Pharmacy, University of North Carolina at Chapel Hill, Chapel Hill, North Carolina 27599,* *United States;* ⦿ orcid.org/0000-0003-4779-9932; Email: alison.axtman@unc.edu

Authors

Frances M. Bashore − *Structural Genomics Consortium (SGC), UNC Eshelman School of Pharmacy, University of North Carolina at Chapel Hill, Chapel Hill, North Carolina 27599, United States;* ⦿ orcid.org/0000-0003-4241-9873

Sophia M. Min − *Structural Genomics Consortium (SGC), UNC Eshelman School of Pharmacy, University of North Carolina at Chapel Hill, Chapel Hill, North Carolina 27599, United States;* ⦿ orcid.org/0000-0001-9840-2996

Xiangrong Chen − *Centre for Medicines Discovery, Nuffield Department of Medicine, University of Oxford, Oxford OX3 7FZ, U.K.*

Stefanie Howell − *Structural Genomics Consortium (SGC), UNC Eshelman School of Pharmacy, University of North Carolina at Chapel Hill, Chapel Hill, North Carolina 27599, United States*

Caroline H. Rinderle − *Department of Microbiology, Immunology and Genetics, University of North Texas Health Science Center, Fort Worth, Texas 76107, United States*

Gabriel Morel − *Kinases and Brain Development Laboratory, The Francis Crick Institute, London NW1 1AT, U.K.*

Josie A. Silvaroli − *Division of Pharmaceutics and Pharmacology, College of Pharmacy and Comprehensive Cancer Center, The Ohio State University, Columbus, Ohio 43210, United States*

Carrow I. Wells − *Structural Genomics Consortium (SGC), UNC Eshelman School of Pharmacy, University of North Carolina at Chapel Hill, Chapel Hill, North Carolina 27599, United States;* ⦿ orcid.org/0000-0003-4799-6792

Bruce A. Bunnell − *Department of Microbiology, Immunology and Genetics, University of North Texas Health Science Center, Fort Worth, Texas 76107, United States*

David H. Drewry − *Structural Genomics Consortium (SGC), UNC Eshelman School of Pharmacy and UNC Lineberger Comprehensive Cancer Center, School of Medicine, University of North Carolina at Chapel Hill, Chapel Hill, North Carolina 27599, United States;* ⦿ orcid.org/0000-0001-5973-5798

Navjot S. Pabla − *Division of Pharmaceutics and Pharmacology, College of Pharmacy and Comprehensive Cancer Center, The Ohio State University, Columbus, Ohio 43210, United States*

Sila K. Ultanir − *Kinases and Brain Development Laboratory, The Francis Crick Institute, London NW1 1AT, U.K.*

Alex N. Bullock − *Centre for Medicines Discovery, Nuffield Department of Medicine, University of Oxford, Oxford OX3 7FZ, U.K.;* ⦿ orcid.org/0000-0001-6757-0436

Complete contact information is available at:
https://pubs.acs.org/10.1021/acsmedchemlett.4c00219

Notes

The authors declare no competing financial interest.

■ ACKNOWLEDGMENTS

■ ABBREVIATIONS USED

IC_{50}, half-maximal inhibitory concentration; NanoBRET, bioluminescence resonance energy transfer using NanoLuciferase; nLuc, NanoLuciferase; nM, nanomolar; PoC, percent of control; PDB, Protein Data Bank; SEM, standard error of the mean

■ REFERENCES

(1) Chowdhury, I.; Dashi, G.; Keskitalo, S. CMGC Kinases in Health and Cancer. *Cancers* **2023**, *15* (15), 3838.

(2) Sassa, T.; Gomi, H.; Sun, W.; Ikeda, I.; Thompson, R. F.; Itohara, S. Identification of Variants and Dual Promoters of Murine Serine/Threonine Kinase KKIAMRE. *J. Neurochem* **2000**, *74* (5), 1809−1819.

(3) Sassa, T.; Gomi, H.; Itohara, S. Postnatal expression of Cdkl2 in mouse brain revealed by LacZ inserted into the Cdkl2 locus. *Cell Tissue Res.* **2004**, *315* (2), 147−156.

(4) Gomi, H.; Sassa, T.; Thomson, R.; Itohara, S. Involvement of cyclin-dependent kinase-like 2 in cognitive function required for contextual and spatial learning in mice. *Front Behav Neurosci* **2010**, *4*, 17.

(5) Fang, C.-L.; Uen, Y.-H.; Chen, H.-K.; Hseu, Y.-C.; Lin, C.-C.; Hung, S.-T.; Sun, D.-P.; Lin, K.-Y. Loss of cyclin-dependent kinase-like 2 predicts poor prognosis in gastric cancer, and its overexpression suppresses cells growth and invasion. *Cancer Med.* **2018**, *7* (7), 2993−3002.

(6) Chen, Z.; Lv, Y.; He, L.; Wu, S.; Wu, Z. Decreased CDKL2 Expression in Clear Cell Renal Cell Carcinoma Predicts Worse Overall Survival. *Front Mol. Biosci* **2022**, *8*, No. 657672.

(7) Taglienti, C. A.; Wysk, M.; Davis, R. J. Molecular cloning of the epidermal growth factor-stimulated protein kinase p56 KKIAMRE. *Oncogene* **1996**, *13*, 2563−2574.

(8) Ruan, B.; Feng, X.; Chen, X.; Dong, Z.; Wang, Q.; Xu, K.; Tian, J.; Liu, J.; Chen, Z.; Shi, W.; Wang, M.; Qian, L.; Ding, Q. Identification of a Set of Genes Improving Survival Prediction in Kidney Renal Clear Cell Carcinoma through Integrative Reanalysis of Transcriptomic Data. *Dis. Markers* **2020**, *2020*, No. 8824717.

(9) Shao, Q.; Wang, F.; Xu, Y.; Zhang, X.; Tang, W.; Feng, Y.; Li, Y. CDKL2 Is Associated with HER2 Status and Overall Survival in Gastric Cancer: Comparative Analysis of CDKL2 Protein Expression and Gene Copy Number. *Biomed Res. Int.* **2020**, *2020*, No. 1712723.

(10) Lin, K. Y.; Uen, Y. H. Loss of CDKL2 expression correlates with differentiation, stage, and poor prognosis of gastric cancer. *Ann. Oncol* **2017**, *28*, x12.

(11) Zhou, Y.; Qiu, X. P.; Li, Z. H.; Zhang, S.; Rong, Y.; Yang, G. H.; Fang, Z. Clinical significance of aberrant cyclin-dependent kinase-like 2 methylation in hepatocellular carcinoma. *Gene* **2019**, *683*, 35−40.

(12) Yi, R.; Yang, S.; Liao, Y.; Hu, Z.; Long, H.; Zeng, Y.; Wang, X.; Qiu, C.; Xu, A.; Lin, J.; Wu, Z. Decreased CDKL2 expression is correlated with the progression and poor prognosis of glioma. *Pathol Res. Pract* **2020**, *216* (5), No. 152920.

(13) Rubicz, R.; Zhao, S.; Geybels, M.; Wright, J. L.; Kolb, S.; Klotzle, B.; Bibikova, M.; Troyer, D.; Lance, R.; Ostrander, E. A.; Feng, Z.; Fan, J.-B.; Stanford, J. L. DNA methylation profiles in African American prostate cancer patients in relation to disease progression. *Genomics* **2019**, *111* (1), 10−16.

(14) Li, L.; Liu, C.; Amato, R. J.; Chang, J. T.; Du, G.; Li, W. CDKL2 promotes epithelial-mesenchymal transition and breast cancer progression. *Oncotarget* **2014**, *5* (21), 10840−10853.

(15) Lindqvist, B. M.; Wingren, S.; Motlagh, P. B.; Nilsson, T. K. Whole genome DNA methylation signature of HER2-positive breast cancer. *Epigenetics* **2014**, *9* (8), 1149−1162.

(16) Bonifaci, N.; Górski, B.; Masojć, B.; Wokołorczyk, D.; Jakubowska, A.; Dębniak, T.; Berenguer, A.; Serra Musach, J.; Brunet, J.; Dopazo, J.; Narod, S. A.; Lubinski, J.; Lazaro, C.; Cybulski, C.; Pujana, M. A. Exploring the Link between Germline and Somatic Genetic Alterations in Breast Carcinogenesis. *PLoS One* **2010**, *5*, No. e14078.

(17) Shen, J.; LeFave, C.; Sirosh, I.; Siegel, A. B.; Tycko, B.; Santella, R. M. Integrative epigenomic and genomic filtering for methylation markers in hepatocellular carcinomas. *BMC Med. Genomics* **2015**, *8* (1), 28.

(18) Zheng, Y.; Huang, Q.; Ding, Z.; Liu, T.; Xue, C.; Sang, X.; Gu, J. Genome-wide DNA methylation analysis identifies candidate epigenetic markers and drivers of hepatocellular carcinoma. *Brief Bioinform* **2018**, *19*, bbw094.

(19) Gomi, H.; Sun, W.; Finch, C. E.; Itohara, S.; Yoshimi, K.; Thompson, R. F. Learning Induces a CDC2-Related Protein Kinase, KKIAMRE. *J. Neurosci.* **1999**, *19* (21), 9530−9537.

(20) Zhao, Y.; Yang, J.; Liu, Y.; Fan, J.; Yang, H. HSV-2-encoded miRNA-H4 Regulates Cell Cycle Progression and Act-D-induced Apoptosis in HeLa Cells by Targeting CDKL2 and CDKN2A. *Virol Sin* **2019**, *34* (3), 278−286.

(21) Canning, P.; Park, K.; Gonçalves, J.; Li, C.; Howard, C. J.; Sharpe, T. D.; Holt, L. J.; Pelletier, L.; Bullock, A. N.; Leroux, M. R. CDKL Family Kinases Have Evolved Distinct Structural Features and Ciliary Function. *Cell Rep* **2018**, *22* (4), 885−894.

(22) Wells, C.; Couñago, R. M.; Limas, J. C.; Almeida, T. L.; Cook, J. G.; Drewry, D. H.; Elkins, J. M.; Gileadi, O.; Kapadia, N. R.; Lorente-Macias, A.; Pickett, J. E.; Riemen, A.; Ruela-de-Sousa, R. R.; Willson, T. M.; Zhang, C.; Zuercher, W. J.; Zutshi, R.; Axtman, A. D. SGC-AAK1−1: A Chemical Probe Targeting AAK1 and BMP2K. *ACS Med. Chem. Lett.* **2020**, *11* (3), 340−345.

(23) Salentin, S.; Schreiber, S.; Haupt, V. J.; Adasme, M. F.; Schroeder, M. PLIP: fully automated protein-ligand interaction profiler. *Nucleic Acid Res.* **2015**, *43* (W1), W443−447.

(24) Silvestre, M.; Dempster, K.; Mihaylov, S. R.; Claxton, S.; Ultanir, S. K. Cell type-specific expression, regulation and compensation of CDKL5 activity in mouse brain. *Mol. Psychiatry* **2024**. DOI: DOI: 10.1038/s41380-024-02434-7.

(25) Castano, A.; Silvestre, M.; Wells, C. I.; Sanderson, J. L.; Ferrer, C. A.; Ong, H. W.; Lang, Y.; Richardson, W.; Silvaroli, J. A.; Bashore, F. M.; Smith, J. L.; Genereux, I. M.; Dempster, K.; Drewry, D. H.; Pabla, N. S.; Bullock, A. N.; Benke, T. A.; Ultanir, S. K.; Axtman, A. D. Discovery and characterization of a specific inhibitor of serine-threonine kinase cyclin-dependent kinase-like 5 (CDKL5) demonstrates role in hippocampal CA1 physiology. *eLife* **2023**, *12*, No. e88206.

(26) Weiss, W. A.; Taylor, S. S.; Shokat, K. M. Recognizing and exploiting differences between RNAi and small-molecule inhibitors. *Nat. Chem. Biol.* **2007**, *3* (12), 739−744.

(27) Matossian, M. D.; Chang, T.; Wright, M. K.; Burks, H. E.; Elliott, S.; Sabol, R. A.; Wathieu, H.; Windsor, G. O.; Alzoubi, M. S.;

King, C. T.; Bursavich, J. B.; Ham, A. M.; Savoie, J. J.; Nguyen, K.; Baddoo, M.; Flemington, E.; Sirenko, O.; Cromwell, E. F.; Hebert, K. L.; Lau, F.; Izadpanah, R.; Brown, H.; Sinha, S.; Zabaleta, J.; Riker, A. I.; Moroz, K.; Miele, L.; Zea, A. H.; Ochoa, A.; Bunnell, B. A.; Collins-Burow, B. M.; Martin, E. C.; Burow, M. E. In-depth characterization of a new patient-derived xenograft model for metaplastic breast carcinoma to identify viable biologic targets and patterns of matrix evolution within rare tumor types. *Clin Transl Oncol* **2022**, *24* (1), 127−144.

(28) Murayama, T.; Gotoh, N. Patient-Derived Xenograft Models of Breast Cancer and Their Application. *Cells* **2019**, *8* (6), 621.